RSC Advances

ROYAL SOCIETY OF CHEMISTRY

www.rsc.org/advances

Preparation of anti-corrosion superhydrophobic coatings by Fe-based micro/nano composite electro-brush plating and blackening process

Yan Wei, Liu Hongtao*, Zhu Wei

College of Materials Science and Engineering, China University of Mining and Technology, Jiangsu, Xuzhou, 221116, P.R. China

Abstract

Superhydrophobic coatings with high strength and corrosion resistance on hard metal surface have been attracting significant attention in recent years. In this paper, a quick and easy method using Fe-based micro/nano composite electro-brush plating and subsequent modification with stearic acid was established for fabricating superhydrophobic surfaces on A3 steel plates. The processing parameters including working voltage, brushing speed and micro-TiO_2 particle concentration were studied to determine their influences on wettability. Blackening process was conducted to further improve the corrosion resistance of Fe-based plating layer with high water repellency. Surface morphology and chemical composition were analyzed by scanning electron microscopy (SEM) and energy disperse spectroscopy (EDS). Corrosion resistance ability was measured by electrochemical workstation. The results suggested that: the rough structure of superhydrophobic coatings can be successfully fabricated by electro-brush plating technology with appropriate parameters; after post-treatment by stearic acid, the contact angle of composite coating was up to 156° and the sliding angle even as low as 1° under the optimal process; meanwhile blackening treated superhydrophobic coatings still maintaining excellent superhydrophobicity and the self-corrosion potential improves by 0.116 V compared to untreated brush plating layer; and the prepared superhydrophobic coatings achieved an excellent long term anti-corrosion performance.

Keywords: superhydrophobic coating corrosion resistance micro /nano composite electro-brush plating blackening treated

1. Introduction

In the field of surface science and engineering, superhydrophobic surfaces[1] have received significant attention and extensive studies because of their excellent performance, including self-cleaning[2], oil-water separation[3], anti-corrosion[4], drag-reduction[5], anti-icing[6], etc. Superhydrophobic surfaces are widely existed in nature, such as lotus and watermelon leaves[7-8], water strider legs[9], butterfly wings, many researchers investigated the characteristics of lotus leaf and found its superhydrophobicity determined by the interaction of micro/nano-structures and low surface energy waxy material[8,10-13]. This discovery provided such model of

preparations of biomimetic superhydrophobic surfaces on many substrates. The surfaces wettability are classified into two major states: Wenzel[13-14] and Cassie-Baxter[15] models. For rough surfaces, they play an important guiding role in studying the wetting mechanism that provides theoretical basis for designing and preparing superhydrophobic surfaces. The micro structures and low surface energy material are the main considerations to manufacture superhydrophobic surfaces. Therefore there are two ways to make surfaces superhydrophobic: One is to fabricate micro/nano roughness directly on the low surface energy material substrate such as Polytetrafluoroethylene, fluorides, etc[16-18]; and the other is to modify a rough surface by materials with low surface energy[19-20].

Carbon steel is the most important and extensively used structure material for its outing performance such as high strength and toughness, easy processing and low-cost. However the poor corrosion resistance of Fe inherently restricts its practical and potential applications greatly[21]. Water is the main factor causing steel rust, therefore, superhydrophobic surface is an ideal choice to achieve non-wetting properties solving the problem of iron rusts in humid environment. For the maintenance of steel facilities in harsh environments, it would reduce billions of dollars to companies as well as governments, if the technology can be applied to buildings, bridges and industrial equipment surfaces made with iron material. Song et al.[22] fabricated superhydrophobic PEEK/PTFE composite coating by changing the curing temperature on 45 steel, the contact angle was up to 161°. MA Frank et al. [23] achieved a superhydrophobic surface on stainless steel by changing the morphology with a sandblasting process and then modifying the low surface energy with myristic acid. Huang et al.[24] designed a superhydrophobic TiO_2-nanotube-coated 316L stainless steel with low adhesion and high corrosion resistance. Some extra methods have also been reported for fabricating superhydrophobic surfaces, including template extrusion[25], emulsion[26], sol-gel processing[27], chemical etching[28], electrospinning[29] etc. However there are some deficiencies such as low mechanical strength, high cost, and the sophisticated preparing process, therefore it is very desirable and promising to develop a facile and efficient method for preparing superhydrophobic surfaces with high strength and low cost on hard metal substrate.

Herein we present a simple and economic micro/nano composite electro-brush plating approach to create a rough coating on hard metal and then blackening processed to prepare superhydrophobic surface with high strength and corrosion resistance. The influences of working voltage, brushing speed and micro-TiO_2 particle concentration on coating wettability and microstructure were investigated. Furthermore, we discussed the mechanism of electro-brush plating preparing

superhydrophobic coating, and analyzed the surface wettability and anti-corrosion performance after blackening treatment.

2. experiment

2.1. Materials and surface treatment

First, the commercial A3 steel plates with size of 5 mm × 4 mm × 1 mm were dealt with mechanical polishing by 400#，600#, 800# and 1000# SiC papers to remove the surface oxide layer. After that the specimens were cleaned ultrasonically for 5 min in anhydrous ethanol to remove surface impurities and then put them in a dry box as substrates. The solution for electric-brush plating was prepared as Table 1 and the solution for blackening process was prepared as Table 2. All chemical reagent were supplied by Shantou Xilong Chemical Company Ltd. (China).

2.2. Fabrication of the superhydrophobic coating

The dried substrates were treated with following process: electrical cleaning→ activation→preplating→plating of TiO_2/Cu composite coating. The main parameters of each step as shown in Table 3. Each process once completed, the simple should be rinsed with deionized water to prevent residual bath from contaminating next process. Since the iron coating is so active in acidic environment that quite easy to rust, a neutralization process should be conducted with a lye solution containing 5 g L^{-1} NaOH for 10 minutes as brush plating was completed, and then dried the specimens after rinsed by deionized water. Subsequently the micro/nano scale rough coating achieved superhydrophobic state after immersing in an ethanol solution containing 5 g L^{-1} stearic acid at 60℃for 40min and then transferred to an oven at 60℃for 2 hours.

In order to further improve surface corrosion resistance and appearance quality, the coating was blackening treated at normal temperature for 1~6 minutes. We got a shiny black surface, however its energy was too high, needing to cover a layer of low surface energy materials to obtain superhydrophobic state. Therefore, the blackening treated specimens were immersed in the ethanol solution with a concentration of 5 g L^{-1} stearic acid for about 40 min at 60℃, then dried in an oven at 60□for 2 hours.

Table 1

The brush plating formula:

working procedure	Chemical constituents	Concentration（g L^{-1}）
electrolytic cleaning solutions	NaOH	15
	Na_3PO_4	40
	$NaC_{12}H_{25}SO_4$	0.1

No.2 activation solutions	H_2SO_4 (18.4mol/L)	80
	$(NH_4)_2SO_4$	120
	$NaC_{12}H_{25}SO_4$	0.1
No.3 activation solutions	$Na_3C_6H_5O_7 \cdot 2H_2O$	180
	$NiCl_2 \cdot 6H_2O$	1
	$H_3C_6H_5O_7$	130
	$C_2H_8N_2O_4$	0.1
Preplating solutions	$NiSO_4 \cdot 7H_2O$	400
	$NiCl_2 \cdot 6H_2O$	20
	CH_3COOH	68
	HCl (36%~38%）	20
Micro-TiO2/Nano-Cu composite plating solutions	$FeCl_2$	600
	$C_6H_8O_7$	120
	$NiCl_2$	50
	CH_3COONH_4	40
	$C_2H_8N_2O_4 \cdot H_2O$	2
	Micro-TiO2	20
	Nano-Cu	5
	$NaC_{12}H_{25}SO_4$	0.1

Tab2

Blackening liquid formula:

`

Chemical constituents	Concentration（g L^{-1}）
$CuSO_4 \cdot 5H_2O$	3
$Na_2HPO_4 \cdot 7H_2O$	2
$C_6H_8O_7$	2
$NaC_{12}H_{25}SO_4$	1
Octaphenyl Polyoxyethyiene	1
$Na_2S_2O_3$	8
H_2SeO_3	4

Tab3

The brush plating and blacking process parameters:

working procedure	Voltage(V)	Time(s)	Relative speed(m/min)
electro-cleaning	+8	30	6~8
No2 activation	-10	30	8~10
No3 activation	+12	60	8~10
Preplating	+12	90	7~9
composite plating	+15	120	8~12
blackening process		60~600	

2.3. Superhydrophobic coating characterization

The water contact angle (WCA) and sliding angle (SA) were measured by surface tension instrument (JC2000D2A, China), each sample measured with a 8 μL deionized water drop at five different positions. The morphology and composition of all fabricated surfaces were observed by scanning electronic microscope (SEM, Quanta 250, FEI, America) equipped with an energy dispersive spectroscopy (EDS, Quantax 400-10, Bruker, Germany), operating at an accelerating voltage of 20 kV. The step profiler (DektakXT, Bruker, Germany) was used to evaluate coating roughness. Corrosion resistance ability of superhydrophobic coating was analyzed by potentiodynamic polarization curves acquired by Electrochemical workstation (C350, China) in a 3.5 wt.% of NaCl solution representing the corrosive environment of seawater.

3. Results and discussion

3.1. Influence of different working voltages on superhydrophobic surface properties

The electro-brush plating voltage was experimented with 6 V, 9 V, 12 V, 15 V on the condition that plating solution containing 20 g L^{-1} micro-TiO_2 and 5 g L^{-1} nano-Cu, the remaining parameters operated according to Table 3. It was observed that the larger the voltage, the greater the efficiency of brush plating, and the coating tended to more uniform and stable. However when the brushing voltage reached 15V, the coating generated heat seriously resulting in the binding force between coating and

substrate rapidly reduced, the process became unstable and part of coating peeling off from substrate. With the increase of working voltage, the coating roughness increased from 375 nm for 6V to 1405 nm for 15 V (Fig.1b), and the contact angle gradually increases to 156° meanwhile the sliding angle decreases from 38° to 1° (Fig.1a). When working voltage reached 15 V, the coating achieved optimal superhydrophobic state with contact angle and sliding angle were 156° and 1° after modification with stearic acid. Beads of water began spinning round while water drops on its surfaces. Fig.2 indicates the contact angles and SEM images under different working voltage, with working voltage increasing, the grains size distributed more and more fine. As the prepared coating with working voltage of 6 V, the contact angle and sliding angle were 130° and 38°, respectively. Fig.2a shows the corresponding coating is smooth and uniform, because the micro/nano particles and metal ions gained electronic with slow speed under a low plating voltage, as a consequence, the coating grew slowly and the rough structure was not obvious. Meanwhile the corresponding surface roughness was measured and found the Ra value was only 375 nm in Fig.1b. With the increase of voltage, current density improved, however the energy inhomogeneity stood out in deposition process, leading that the coating surface appeared lots of small homogeneous protrusions[30] as shown in Fig.2b. As working voltages was 12 V, the contact angle increased to 148°, and sliding angle reduced to 9°, a remarkable change in surface morphology was observed from the Fig.2c: the coating became more uneven with more and more micro/nano dual rough structures appearance[31-32], which can be proven by the surface roughness (1176 nm). The apparent contact angle existed as Cassie state when water droplet contact with the rough structure surface. Fig.2d shows an appropriate surface morphology for achieving the best superhydrophobic properties with 15V operating voltage, meanwhile the pore structures tended to more regular with roughness of 1405 nm (Fig.1b) and the grains distributed more uniform and fine shown in Fig.2d. The contact angle was up to 156° and the sliding angle was only 1°, therefore water drops started rolling as soon as they touched the surface, which should be attribute to the rich porosity and rough structure.

3.2. The influence of brush speed on hydrophobic coating properties

Fig.3 shows the relationship between brushing speed and the coating wettability measured by a deionized water of 8 μL. The brushing speed was set as 5 m/min, 9 m/min, 13 m/min, 17 m/min respectively while the remaining parameters and bath composition were kept constant as shown in Table 3 and Table 1, respectively. As the brushing speed was 5 m/min, an uneven coating with a number of granular projections of mountain-like composing of many about1 μm fine grains, which can be shown in Fig. 4a [33-34] and the corresponding roughness was 1136 nm. It possessed high superhydrophobicity with the contact and sliding angle of 151° and 3° respectively.

However, current density was significantly increased due to the lower brush plating speed, which resulted in severe heat production, meanwhile bubbling, corrugation, abscission and cracking were detected on the composite coatings. Fig.4b indicates a homogeneous porous structure under the brushing speed of 9 m/min, its roughness curve (Fig.3b) was quite regular and highly consistent with the surface morphology in Fig.4b. It was difficult to place drops on this surface due to the higher contact angle and lower sliding angle of 152° and 2° respectively, which indicted an ideal brush speed as it is beneficial to micro/nano particles mosaics, nucleation and growth. While brushing speed varied between 5 m/min and 13 m/min, the contact angle fluctuated at 150° (Fig.3), this should be attributed to the high roughness values above 1100 nm. However it is worth noting that when speed was up to 17 m/min, coatings grain deposition and growth time was substantially reduced with metal ions nucleating on the cathode, the grain of Fe became more fine and homogeneous in agreement with the coating topography in Fig.4d, as a consequence, the contact angle was measured and found to be only 146° and sliding angle increased to 15°.

3.3. Influence of micro-TiO_2 particles concentration on the performance of super hydrophobic coating

The effect of different concentrations of micro-TiO_2 on hydrophobic properties was studied by changing the micro-TiO_2 particles content in plating solution. Through experiments, the concentration of TiO_2 particles were fixed to 0 g L^{-1}, 5 g L^{-1}, 10 g L^{-1}, 20 g L^{-1}, 30 g L^{-1} and 40 g L^{-1} while keeping other variables constant as shown in Table 1 and Table 3, respectively. A 8 uL water droplet used to measure the contact angle and sliding angle. It can be seen from the Fig.5a, the contact angle firstly increases from 139° to 156° and then drastically decreases to 138° with increasing of micro-TiO_2 particles content, while the sliding angle decreases firstly and increases subsequently. Fig.5b demonstrates the variation of roughness, with TiO_2 particles increasing, the roughness increased from 467 nm to 1431nm and then decreased to 806 nm, which agreed with the changes of water contact angle. According to SEM images of Fig.6a, it is observed that the coating was relatively flat and detected a few portion of the cauliflower head[35,39] consisting of bulk grain with additive micro-TiO_2 particles of 0 g L^{-1}, the contact angle and surface roughness were measured and found only 139° and 467 nm, respectively. Naturally it was confirmed the coating wettability existed as Wenzel model. As micro-TiO_2 particle was 5 g L^{-1}, the contact angle reached to 145° while appearing more finely projections in Fig.6b, compared with coating preparation of 0 g L^{-1}. When the miro-TiO_2 particles additive was 10 g L^{-1}, the contact angle increased to 150°, sliding angle was less than 10° and the roughness increased to 1031 nm, therefore Cassie state started to dominate the prepared surface, which had achieved superhydrophobic state. Some remarkable

changes are presented in Fig.6c, the porosity scale and proportion dramatically increased, at the same time even more sharp projections[30] can be observed. With the increasing of TiO_2 particles to 20 g L^{-1}, the sliding angle was 2° and water drops were automatically rolling without tilting the test sample, while the maximum value of contact angle for coatings we can measure was 156°, as water drops started rolling as soon as they were placed on the coatings, superhydrophobic coating has achieved the best performance, because of the uniform roughness curve and high Ra (1431 nm). When micro-TiO_2 particles increased to 30 g L^{-1}, a slightly decrease in the contact angle value at 151°, the corresponding rolling angle increased to 7° which should be attributed to coatings poor porosity and protrusion (Fig.5e), meanwhile surface roughness reduced to 1076 nm as shown in Fig.4b. It is clearly that coatings grains becoming more fine and some regions appearing grain reunion[33-34] due to high sticky bath for poor wrapping capability and conductivity causing by the excess miro-TiO_2 particles. However, when TiO_2 particles was 40 g L^{-1}, the SEM images of Fig.5f indicates: the morphology of coating has undergone a tremendous change, lots of tiny grains created a larger aggregates, which was similar to a flower cluster with diameter about 10μm, the uniform convex structure was disappeared and coating roughness obtained only 806 nm and the spacing of some protruding tended to be wilder in roughness curve quite fitting in the morphology in Fig.5f. The contact angle was measured and found to be 138° while the sliding angle was 29° and water droplets are hard to scroll. This mainly due to an excess of micro-TiO_2 particles resulting in a sticky bath, metal ions can be hardly flow freely, causing severe reunion over the particles deposition.

3.4. The mechanism of the electro-brush plating to prepare superhydrophobic coating

The optimal superhydrophobic coating was investigated by EDS to analyze surface composition, as can be seen from Fig.7a, there are five different peaks, representing the coating were consist of element Fe, Ti, O, Ni and Cu, which was consistent with the chemical composition of the plating solution. The elements of Ti and O came from micro-TiO_2 particles that embedded in the coating surface during plating process. The Cu element on coating surface partly from the exposed nano-Cu particles of the plating layer, partly due to plating tip effect that a large amount of nano-Cu transformed into copper ions in the process of nucleation and growth, which was to restore to elemental copper priority[35-36]. From the coating EDS map of each element distribution in Fig.7b, it indicates that the micro/nano-particles and metal ions of solution have occurred co-deposition successfully[37-40]. The Nano-Cu particle in electrodeposition process was mainly contributing to increase the conductivity and current density of bath, at the same time with synergies of micron-TiO_2 as nucleation of composite coating to improve the nucleation rate[37]. Due to intermittent

electrodeposition at a high current density, the cathode surface was always in an unstable state, coupled with the cutting-edge effect of micro-nano particles, forming a rough and porous structure. This feather was very helpful for storing air to form a cushion holding water droplets, after modifying with stearic acid, the optical image of water droplets on this structure coating as shown in Fig.8a. The coating convexo/ concave structure was observed by scanning electron microscopy and it could be simplified into a model as shown in Fig.8b. The micro /nano roughness and porosity can catch a lot of air forming an air cushion, as a result that water can not enter into the coating holes and voids, obtaining superhydrophobic state. According to water droplets in the liquid, solid and gas three-phase composite surface proposed by Cassie, contact angle calculation formula can be expressed as [13]:

$$\cos\theta_c = f_1 * \cos\theta - f_2$$

where θ_c is the apparent contact angle of roughness surface, θ is the apparent contact angle of the smooth surface, f_1 is the percentage of droplets with a solid surface occupied by the composite interface, f_2 is the percentage of water droplets in contact with the air interface ($f_1 + f_2 = 1$). By measuring the A3 smooth surface and micro/nano composite coating give the contact angle at 96° and 156°, respectively. It can be calculated that the f_2 is 0.9035, obviously the air in the proportion of compound contact interface as high as 90.35%.

3.5. The morphology and composition of blackening treated composite coating

In order to further improve the corrosion resistance and surface aesthetics for coating while maintaining excellent superhydrophobicity, blackening process at room temperature is an ideal choice. The morphology and composition of blackening treated coating were determined by SEM and EDS, the results can be shown in Fig.9. According to SEM image(Fig.9a), it is found that the rough structure has not been destroyed in blackening process, still keeping rough geometric features, this kind of convex-concave structures were inherited from the previous composite coating. As can be seen from EDS spectra, it is detected seven different peaks, demonstrating the chemical composition of blackening processed coatings are consist of elements Cu, Se, P, S, Fe, C and O, which are consistent with the chemical composition of blackening liquid. According to relevant literature[41-42] and combined the analysis of SEM image and EDS spectra, it is considered that compositions of black film might be mainly consist of CuSe and FeSe, after post-treated by ocatadecanoic acid, the contact

angle of blackening treated composite coating was up to 156°, sliding angle was less than 3°, exhibiting excellent water repellency.

3.6. Mechanical stability

The mechanical stability of superhydrophobic surface is one of the key considerations for its practical applications. Scratch and tape-peeling tests are regarded as effective ways to evaluate the mechanical abrasion resistance. The pressure to press the tape to the sample is the "finger press" as described in the standard ASTM D 3359-09$^{\varepsilon 2}$. The blacking treated coating can resist tape peeling 60 times by Scotch-600 adhesive tape. While the Fe-based composite coatings only survive 30 peeling times with contact angle and sliding angle of 150° and 8°. Therefore, the blacking treated surface achieves a better superhydrophobicity and higher binding force compared to the Fe-based composite coatings.

The schematic diagram of scratch test as shown in Fig.10a. We adopt 800 grit SiC sandpaper as an abrasion surface and load different weight on the sample. The testing contact area is 10 mm × 15 mm. Fig. 10b indicates that the blacking treated surface and Fe-based composite coatings still keep superhydrophobic ability with contact angle above 150° and sliding angle below 10° after abrasion for 80 cm under 4 kPa pressure. As the sliding distance increases to 1.2 m, the Fe-based composite coatings loss its superhydrophobicity, while the blacked sample could survive 1.4 m. Fig.10c shows the variation of water contact angle and sliding angle under different pressure with a sliding distance of 0.8 m. With the increase of pressure, the contact angle is diminished gradually and the sliding angle becomes larger. The Fe-based composite coating firstly lose its superhydrophobicity with a pressure of 5 kPa, and with the further increasing pressure, the contact angle of blacking treated surface deceases to 143° and superhydrophobicity is failed as well. While the mechanical abrasion resistance of as prepared coatings achieve much better than previous reports: the superhydrophobicity of magnesium alloy is lost after 70 cm of abrasion on 800 grid sandpaper at an applied pressure of 1.2kPa[43]; after 25cm of abrasion under 3.45kPa pressure, the superhydrophobicity of the Si surface disappeared[44]. The SEM image of the samples after abrasion for 1 m at 5 kPa are displayed in Fig.12. The Fe-based composite coatings There are some scratches covering the coating and a portion of the micro structures are damaged in abrasion test(Fig.12a). The blacking treated surface seems to be damaged more severely than Fe-based composite coatings, however it still exhibits an excellent superhydrophocity, this due that the blacking treated surface has much more porous and microscale structures, leading the distribution of low surface energy material is more dense and uniform covering the coating.

3.7. The comparison of corrosion resistance with the A3 steel substrate, blackening treated A3 steel substrate, Fe-based composite coatings and blackening treated Fe-based composite coatings

The potentiodynamic polarization curve was carried out using electrochemical workstation to investigate anti-corrosion performance. First, the A3 steel substrate, blackening treated A3 steel substrate, Fe-based composite coatings and blackening treated Fe-based composite coatings were soaked in 3.5% NaCl corrosion solution stabilizing for 1 hour, then measured the potentiodynamic polarization curves by electrochemical workstation. SEC electrod was used as reference electrode, Pt electrode as auxiliary electrode, working electrode was the prepared samples with 10mm×10mm exposed area. The polarization curve of different treated samples are shown in Fig.12, according to the fitting tafel curves and Table 4, the A3 steel corrosion potential(E_{corr}) and corrosion current density (I_{corr}) are -0.689V and 1.04×10^{-4} A.cm^{-2}, respectively. Whereas the E_{corr} and I_{corr} of blackening treated A3 steel substrate are -0.551V and 1.96×10^{-5} A·cm^{-2}, it is obvious that the blacking film can effectively improves the steel substrate corrosion resistance. The anti-corrosion property of Fe-based composite coatings is further improving with E_{corr} and I_{corr} values at -0.443V and 9.19×10^{-6} A·cm^{-2}. After blackening process, the superhydrophobic coating achieved its best corrosion resistance, corrosion potential decreased to -0.33V, corrosion current density as low as 3.21×10^{-6} A·cm^{-2}, its corrosion potential is more positive and corrosion current density much lower than A3 steel substrate, because the superhydrophobic surface coating has a lotus-like micro structure, water droplets can be alienated to the surface, so the contact area between water droplets and superhydrophobic surface is tiny, the superhydrophobic surface could effectively reduce the extent of corrosion. It is worth noting that the blackening treated composite coating is significantly positive compared to both superhydrophobic coating and A3 steel substrate as shown in Fig.12. While the corrosion resistance of blackening treated A3 steel substrate without superhydrophobicity just have a slight improvement. Fig.13a-b. shows the morphology of blacking treated samples, it is clear that there are only some minor micro structures on A3 steel substrate lacking of the structures of convex and holes compared to blacking treated Fe-based composite coating, which can be proved by the two samples surface roughness shown in Fig.13c. Therefore, the wettability of blacking treated A3 steel substrate was composed of Wenzel and Cassie composite states, leading NaCl solution immersed in the coating with a poor anti-corrosion property. The deposition film of stable CuSe played an important role to improved the electrochemical stability in corrosive environment, making self-corrosion potential moved to positive direction.

Table 4

The corrosion potential (E_{corr}) and the corrosion current density(I_{corr}) of A3 steel substrate, blacking treated A3 steel substrate, Fe-based composite coating and the blacking treated Fe-based

composite coating in 3.5% NaCl solution.

Sample	E_{corr} (V)	I_{corr} ($A \cdot cm^{-2}$)
A3 steel substrate	-0.689	1.04×10^{-4}
Blacking treated A3 steel substrate	-0.551	1.96×10^{-5}
Fe-based composite coating	-0.443	9.19×10^{-6}
Blacking treated Fe-based composite coating	-0.327	3.21×10^{-6}

The long term corrosion test in 3.5% NaCl solution was conducted and the results is shown in Fig.14 (A). It is clear that the blacking treated coating and Fe-based composite coating achieve a better long term anti-corrosion performance compared to A3 steel substrate. With the increase of immersion time, the open circuit potential of coated samples is decreased at first, then trend to stable at -0.6V and -0.55V, respectively. It should be attributed the wettability change from superhydrophobic to hydrophilic state. However the A3 steel substrate potential is more negative that due to lake of the protection of composite coating and blacking film.

The optical images of the A3 steel substrate, Fe-based composite coatings and blacking treated surface substrates after staying in 3.5% NaCl solution for several days can be seen in Fig.14B. It is clear that the A3 steel substrate indicates a poor anti-corrosion performance with the increasing of immersion time compared to the two superhydrophobic sample. Fig.14B-a shows the corrosion is firstly appeared in the A3 steel surface and solution changes from clear to a rust-color after staying in 3.5% NaCl for 2 day, whereas the superhydrophobic substrates still keep their original state and the solution of immersing Fe-based composite coatings and blacking treated surface still remain clear and transparent. As the immersion time increases to 7 days, a small area of corrosion appeared in the Fe-based composite coatings, however the blacking treated surface could only be found a small amount of rust until immersing for 14 days in 3.5% NaCl solution(Fig.14B). Therefore, the superhydrophobic blacking treated coating could provide a long-term protection for A3 steel. Meanwhile the corresponding EIS can be seen in Fig.14B(d-f). Fig.B-d shows the corrosion is firstly appeared in the A3 steel surface and solution change shows the impedance values of A3 steel substrate, Fe-based composite coatings and blacking treated surface

substrates immersion for 0 day, due to the existence of air film between water and substrate, the superhydrophobic surfaces own a very high impedance compared to A3 steel substrate. After the substrates immersed for 2 days, the impedance of Fe-based composite coatings and blacking treated surface have suffered a great fall because their wettability transform into Wenzel and Cassie composite state from the single Cassie state leading to the weakening of air film effect. When the immersion time increases to 14 days, the impedance of blacking treated surface is around $10000\Omega \cdot cm^{-2}$ that much larger than Fe-based composite coatings ($2000\Omega \cdot cm^{-2}$), this is due to the blacking film have a fine and close texture[45]. However the A3 steel substrate impedance is minimum only about $400\Omega \cdot cm^{-2}$. The excellent anti-corrosion performance of blacking treated coating should be attributed to the combined protection effect of both blacking film and Fe-based composite coatings(Fe-Cu-Ni)[46], Blackening process not only improve its anti-corrosion ability and surface aesthetics but also added the functions of light absorption, anti-reflective, which have a wide application prospect in military products.

4. Conclusions

In summary, a metallic superhydrophobic coating with excellent anti-corrosion performance was fabricated by micro/nano composite electro-brush plating technology and blackening process. We analyzed the processing main factors affecting coating superhydrophobicity and reached some conclusions as following: the anti-corrosion superhydrophobic coating can be successfully prepared on A3 steel by composite brush plating and blackening process with appropriate parameters; when the working voltage is 15 V, brush plating speed is 9 m/min, the concentration of micro-TiO_2 particles is 20 g L^{-1}, nano-Cu particles is 5 g L^{-1}, which are the optimal process parameters for preparing a superhydrophobic surface, the contact angle is up to 156°, the sliding angle is as low as 1° after modifying with stearic acid; the contact angle of blackening processed superhydrophobic coating still remaining 156°, sliding angle is less than 3°. The as prepared coatings exhibit excellent abrasion resistance and the anti-corrosion performance is greatly improved compared with superhydrophobic coating for non-blackening.

Acknowledgment

This work was supported by the National Nature Science Foundation of China (No.51475457) and Qing Lan Project. We express our grateful thanks to them for their financial support.

Reference

[1] A. Lafuma,D. Quere, Superhydrophobic states, Nat. Mater. 2 (2003) 457-460.

[2] R. Blossey, Self-cleaning surfaces-virtual realities, Nat. Mater. 2 (2003) 301.

[3] J. Zhang,S. Seeger, Polyester materials with superwetting silicone nanofilaments for oil/water separation and selective oil absorption,Adv.Funct. Mater. 21 (2011) 4699.

[4] Y.Chen, S.Chen, F.Yu, W.Sun, H.Zhu, Y.Yin, Fabrication and anti-corrosion property of superhydrophobic hybrid film on copper surface and its formation mechanism, Surf. Interface Anal. 41 (2009) 872.

[5] R. Truesdell, A. Mammoli, P. Vorobieff, F. Swol, C.J. Brinker, Drag reduction on a patterned superhydrophobic surface, Phys. Rev. Lett. 97 (2006) 044504.

[6] L. Mishchenko, B. Hatton, V. Bahadur, J.A. Taylor, T. Krupenkin, J. Aizenberg, Design of ice-free nanostructured surfaces based on repulsion of impacting water droplets, ACS Nano. 4 (2010) 7699 – 7707.

[7] C. Extrand, W. Moon, Sung, Repellency of the Lotus Leaf: Contact Angles, Drop Retention, and Sliding Angles, Langmuir. 30 (2004) 8791-8797.

[8] A. Marmur, The lotus effect: Superhydrophobicity and metastability, Langmuir. 20 (2004) 3517–3519.

[9] X. Gao, L. Jiang, Biophysics: water-repellent legs of water striders, Nature 432 (2004), 36-36.

[10] E. Bormashenko, O. Gendelman, G. Whyman, Superhydrophobicity of Lotus Leaves versus Birds Wings: Different Physical Mechanisms Leading to Similar Phenomena, Langmuir. 28 (2012) 14992-14997.

[11] L. Feng, S. Li, Y. Li, H.J. Li, L.J. Zhang, J. Zhai, Y.L. Song, B.Q. Liu, L. Jiang, D.B. Zhu, Super-hydrophobic surfaces: from natural to artificial, Adv. Mater.

[12] P. Roach, J. Shirtcliffe, M. Newton, Progess in superhydrophobic surface development, Soft Matter. 4 (2008) 224-240.

[13] R.N. Wenzel, Resistance of solid surfaces to wetting by water, Ind. Eng. Chem. 28 (1936) 988 – 994.

[14] R.N. Wenzel, Surface roughness and contact angle, J. Phys. Chem. 53 (1949) 1466 – 1467.

[15] A. Cassie, S. Baxter, Wettability of porous surfaces, T. Faraday Soc. 40 (1944) 546 – 551.

[16] W.X. Hou, Q.H. Wang, Stable polytetrafluoroethylene superhydrophobic surface with lotus-leaf structure, J. Colloid & interface. Sci. 333 (2009) 437-443.

[17] D.W. Gong, Y.L. Jiang, P.X. Fan, Thermal stability of micro-nano structures and superhydrophobicity of polytetrafluoroethylenefilms formed by hot embossing via a picosecond laser ablated template, Appl. Surf. Sci. 331 (2015) 437-443.

[18] T.Li, J. He, L. Yao, Z. Geng, Robust antifogging antireflective coatings on polymer substrates by hydrochloric acid vapor treatment. Coll. Interf. Sci. 444 (2015) 67-73.

[19] Z. Chen, F. Tian, A. Hu, M. Li, A facile process for preparing superhydrophobic nickel films with stearic acid, Surf. Coat. Techno 231 (2013) 88-92.

[20] Z. She, Q. Li, Z. Wang, C. Tan, J. Zhou, L. Li, Highly anticorrosion, self-cleaning superhydrophobic Ni-Co surface fabricated on AZ91D magnesium alloy, Surf. Coat. Techno. 251 (2014) 7-14.

[21] B. Panda, R. Balasubramaniam, G. Dwivedi, On the corrosion behaviour of novel high carbon rail steels in simulated cyclic wet-dry salt fog conditions, Corro. Sci. 50 (2008) 1684-1692.

[22] Song Haojie, Zhang Zhaozhu, Men Xuehu. Super-hydrophobic PEEK/PTFE Composite Coating [J]. Appl. Phys. a-Mater. Sci.&Proce. 91 (2008) 73-76.

[23] Frank M A, Boccaccini A R, Virtanen S. A facile and scalable method to produce superhydrophic stainless steel surface [J]. Appl. Surf. Sci. 311 (2014) 753 – 757.

[24] Q.L. Huanga, Yun Yanga, Ronggang Hub, et al. Reduced platelet adhesion and improved corrosion resistance of superhydrophobic TiO_2-nanotube-coated 316L stainless steel [J]. Coll. Surf. B: Biointerfaces. 12 (2015) 134-141.

[25] H.S. Hwang, S.B. Lee, I. Park, Fabrication of Rasp-berry-Like superhydrophobic hollow silica particles, Mater. Lett. 64 (20) (2010) 2159 – 2162.

[26] T. Yang, H. Tian, Y. Chen, Preparation of superhy-drophobic silica films with honeycomb-like structure by emulsion method, J. Sol – Gel Sci. Technol. 49 (2009) 243-246.

[27] S.S. Latthe, H. Imai, V. Ganesan, A.V. Rao, Super-hydrophobic silica films by sol-gel co-precursor method, Appl. Surf. Sci. 256 (1) (2009) 217-222.

[28] K.K. Lau, J. Bico, K.B.K. Teo, M. Chhowalla, G.A.J. Amaratung, W.I. Milne, G.H. McKinley, K.K. Gleason, Superhydrophobic carbon nanotube forests, Nano Lett. 3 (12) (2003) 1701-1705.

[29] M. Ma, Y. Mao, M. Gupta, K.K. Gleason, G.C. Rutledge, Superhydrophobic fabrics produced by electrospinning and chemical vapor deposition, Macro-molecules. 38 (23) (2005)

9742-9748.

[30] E. Bittoun, A. Marmur, Optimizing Super-Hydrophobic Surfaces: Criteria for Comparison of Surface Topographies [J]. Adhension. Sci. Tec. 23 (2009) 401-411.

[31] X.W. Li, C. Wang, Y. Yang, Dual-Biomimetic Superhydrophobic Electrospun Polystyrene Nanofibrous Membranes for Membrane Distillation, ACS. Appl. Mater. Interf. 6 (2014) 2431-2438.

[32] N. Gupta, S. Sasikala, D.B. Mahadik, Dual-scale rough multifunctional superhydrophobic ITO coatings prepared by air annealing of sputtered indium-tin alloy thin films, Appl. Surf. Sci. 258 (2012) 9723-9731.

[33] B. Emami, T. M. Bucher, H. V. Tafreshi, Simulation of meniscus stability in superhydrophobic granular surfaces under hydrostatic pressures, Coll. Surf. A. 385 (2011) 95-103.

[34] M.M. Amrei, H.V. Tafreshi, Effects of hydrostatic pressure on wetted area of submerged superhydrophobic granular coatings, Coll. Surf. A. 465 (2015) 87-98.

[35] Q. Yu, Z. Zeng, W. Zhao, M. Li, X. Wu, Q. Xue, Fabrication of adhesive superhydrophobic Ni-Cu-P alloy coatings with high mechanical strength by one step electrodeposition, Coll. Surf. A. 427 (2013) 1-6.

[36] J.M. Lee, K.M. Bae, K.K. Jung, J.H. Jeong, J.S. Ko, Creation of microstructured surfaces using Cu-Ni composite electrodeposition and their application to superhydrophobic surfaces, App. Surf. Sci. 289 (2014) 14-20.

[37] H. Liu, X. Wang, H. Ji, Fabrication of lotus-leaf-like superhydrophobic surfaces via Ni-based nano-composite electro-brush plating, App. Surf. Sci. 288 (2014) 341-348.

[38] S. Huang, Y. Hu, W. Pan, Relationship between the structure and hydrophobic performance of Ni-TiO_2 nanocomposite coatings by electrodeposition, Surf. Coat. Tech. 205 (2011) 3872-3876.

[39] Y. Qinglong, L. Wendan, L. Ping, Microstructure and Properties of Nicke1-Base Nano-Y_2O_3 Composite Coating Prepared with Electro-brush Plating, Rare Metal Materials and Engineering, 41 (2012) 603-606.

[40] L. Du, B. Xu, S. Dong, H. Yang, Y. Wu, Preparation, microstructure and tribological properties of nano-Al_2O_3/Ni brush plated composite coatings, Surf. Coat. Tech. 192 (2005) 311-316.

[41] Chen, Ze-min. Lu, Pin. Gao, Jing-yin, Preparation and Characterization of Blackening Films in Steel Surface, Adv. Mater. Res. 560 (2012)1084-1087

[42] Zhongcheng, Z, Compound-layer blackening of steel at room temperatures, Plat. Surf. Finish.90 (2003) 49-50.

[43] She Z, Li Q, Wang Z, et al. Researching the fabrication of anticorrosion superhydrophobic surface on magnesium alloy and its mechanical stability and durability[J]. Chemical Engineering Journal, 2013, 228: 415-424.

[44] Xiu Y, Liu Y, Hess D. W, Wong C. Mechanically Robust Superhydrophobicity on Hierarchically Structured Si Surfaces. Nano-technology 2010, 21, 155705.

[45] J. X. Zhang. A New Blacking Process for Stainless Steel. Corrosion & Protection (2008).

[46] Shi, Zhong Ning, et al. "Anti-oxidation and anti-corrosion properties of Ni-Fe-Cu inert metal anodes." Chinese Journal of Nonferrous Metals14.4(2004):591-595.

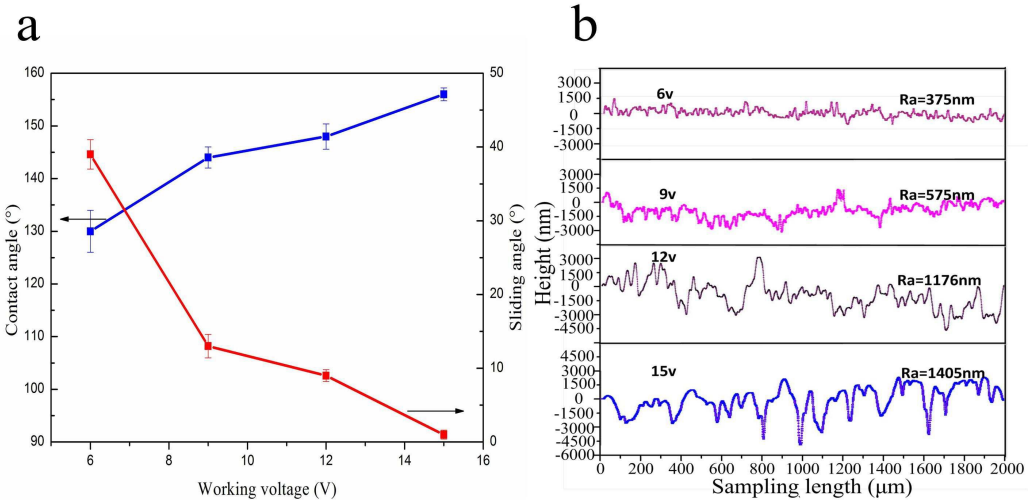

Fig.1a. The contact angle and sliding angle under different working voltage

Fig.1b. The roughness profile curves under different working voltage

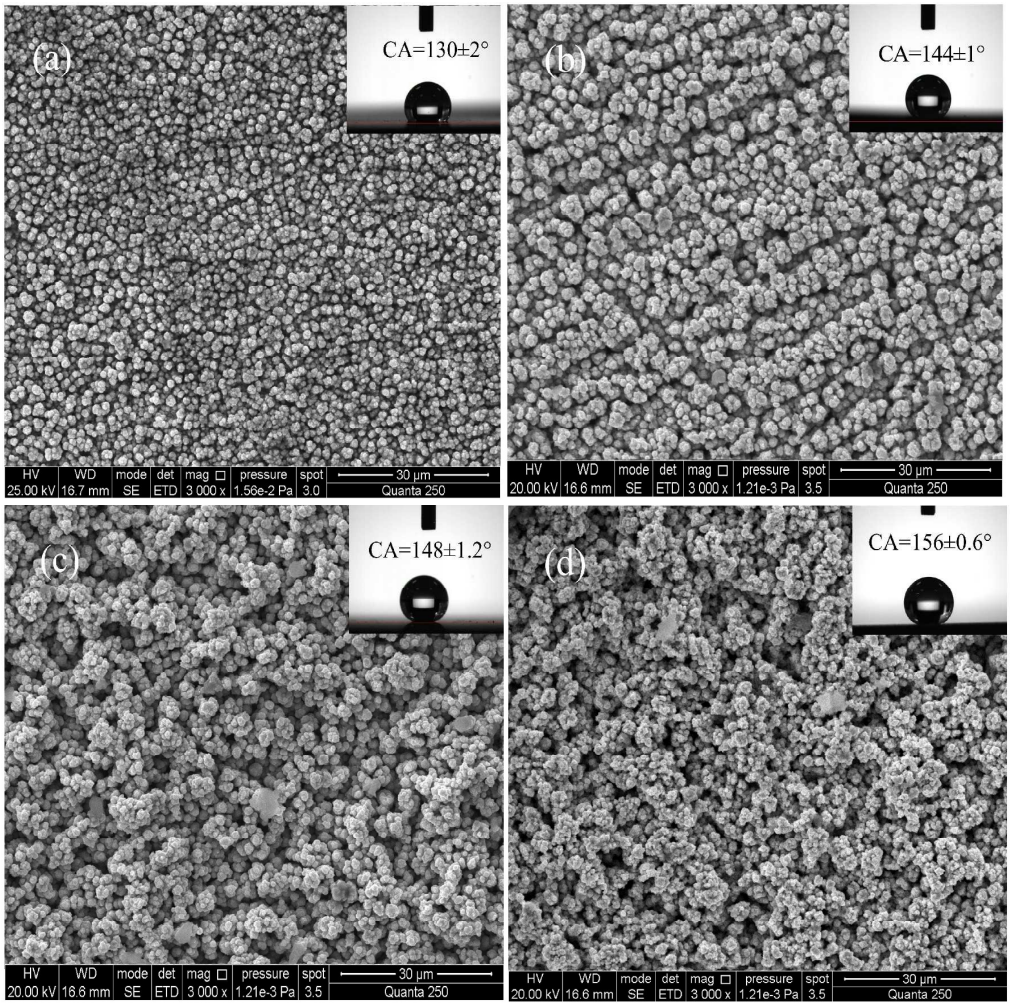

Fig.2.The coating morphology under different working voltage(at 3000×magnifications). (a) 6 V, (b) 9 V, (c) 12 V, (d) 15 V.

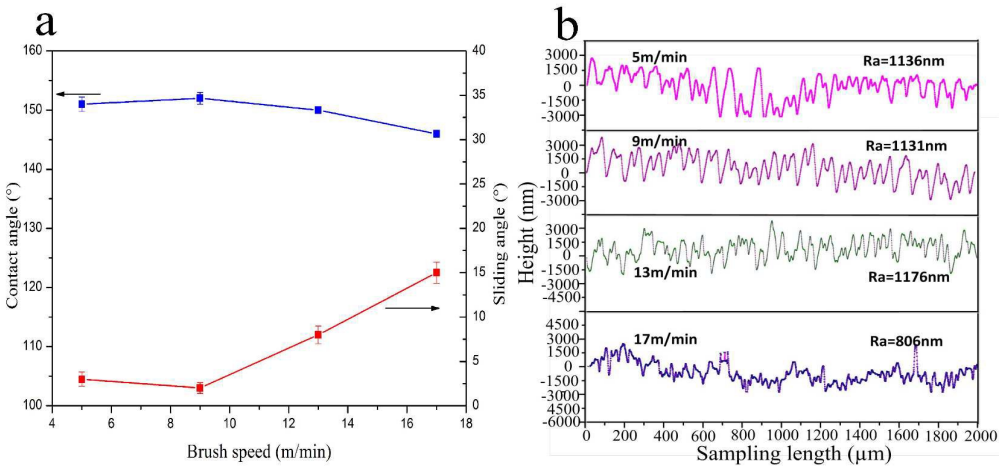

Fig.3a.The contact angle and sliding angle under different brushing speed

Fig.3b. The roughness profile curves under different brushing speed

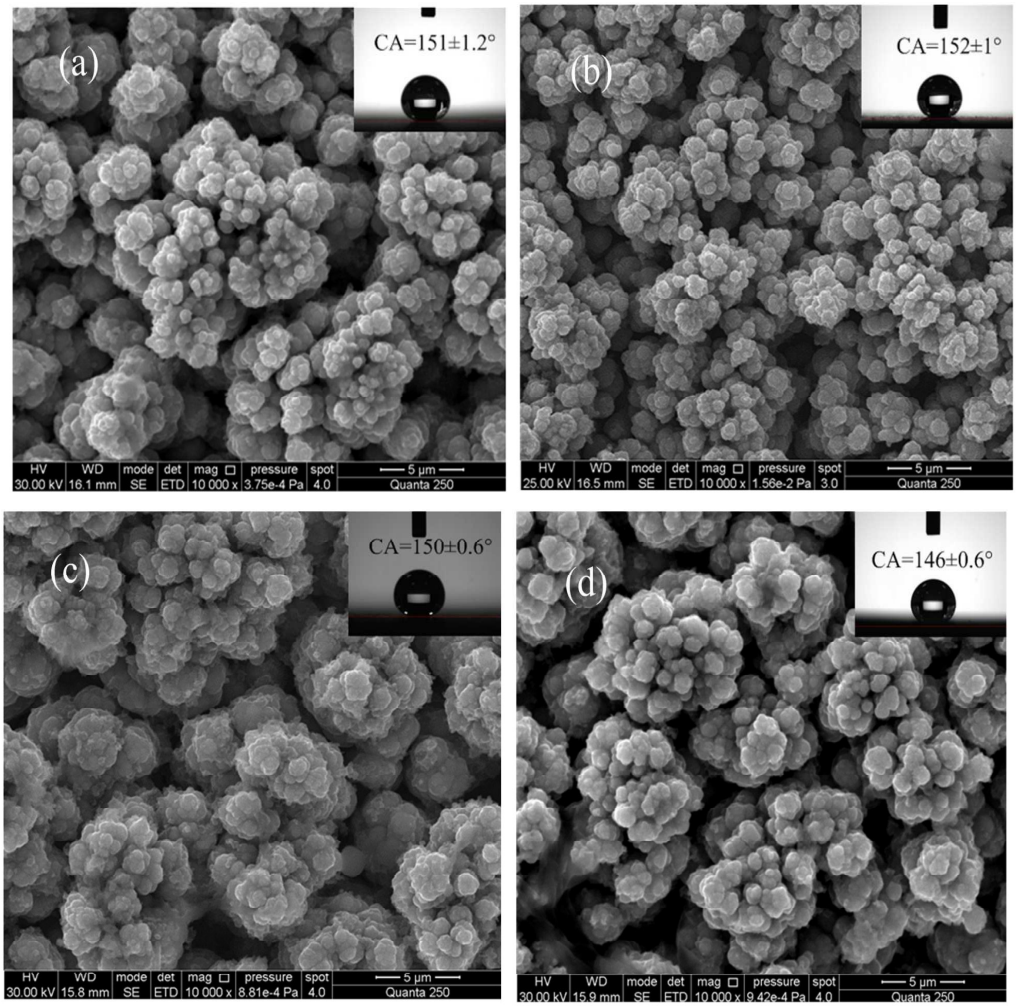

Fig.4.The coating morphology under different brushing speed (at 10000×magnifications). (a) 5 m/min, (b) 9 m/min, (c) 13 m/min, (d) 17 m/min.

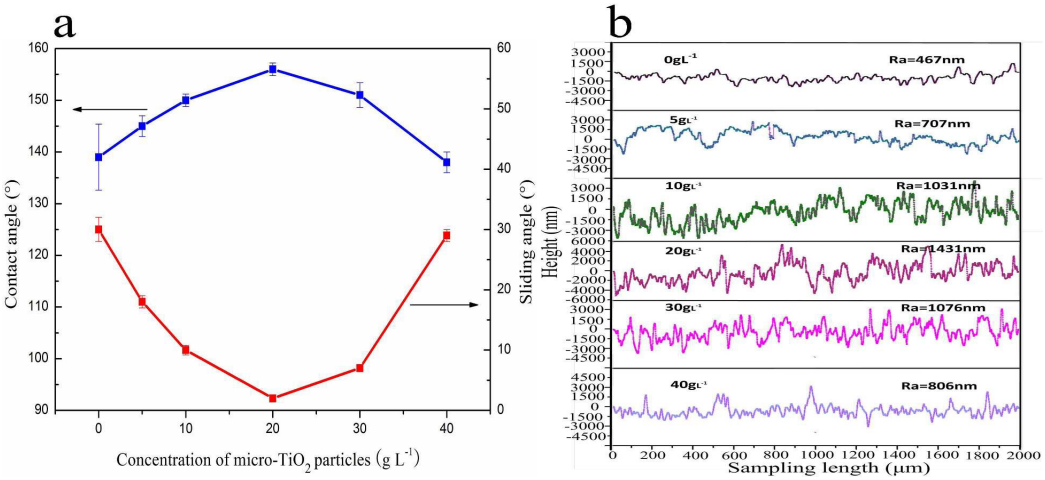

Fig.5a.The contact angle and sliding angle with different micro- TiO_2 particles concentration

Fig.5b. The roughness profile curves with different micro- TiO_2 particles concentration

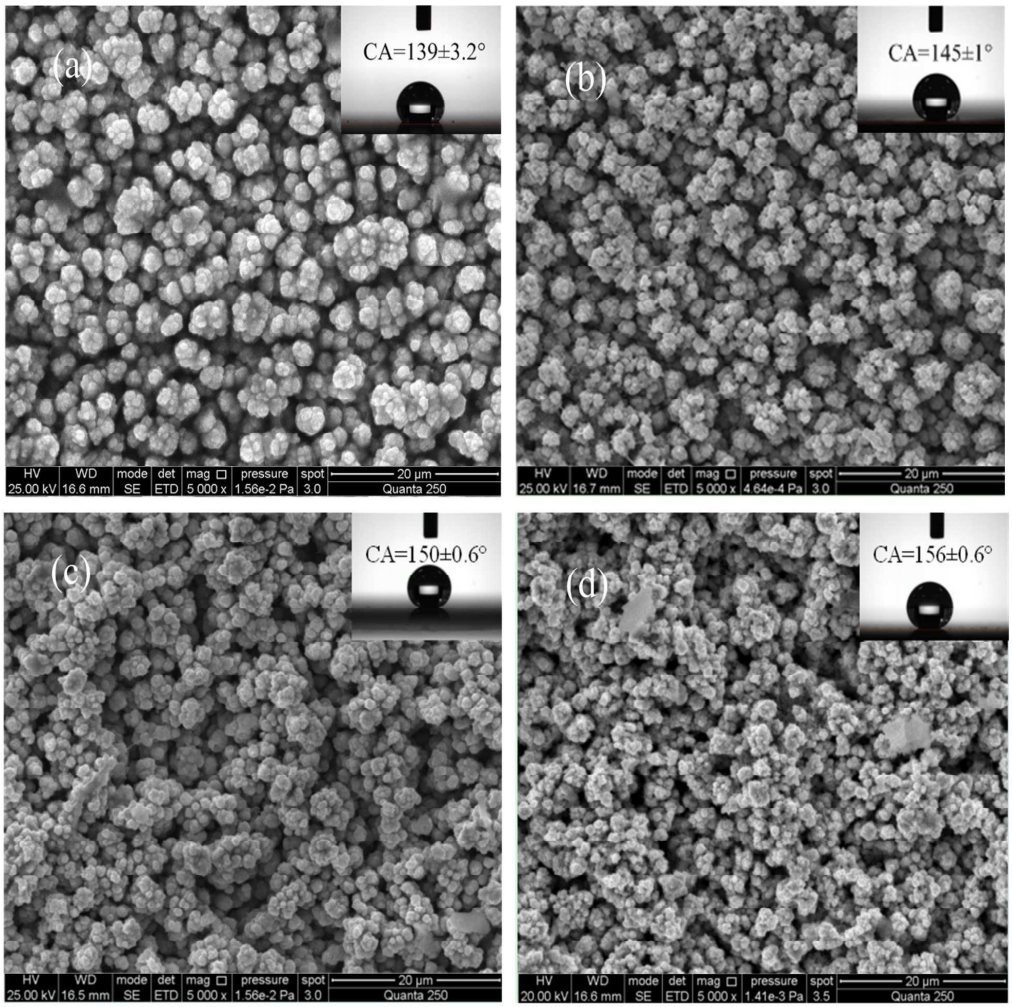

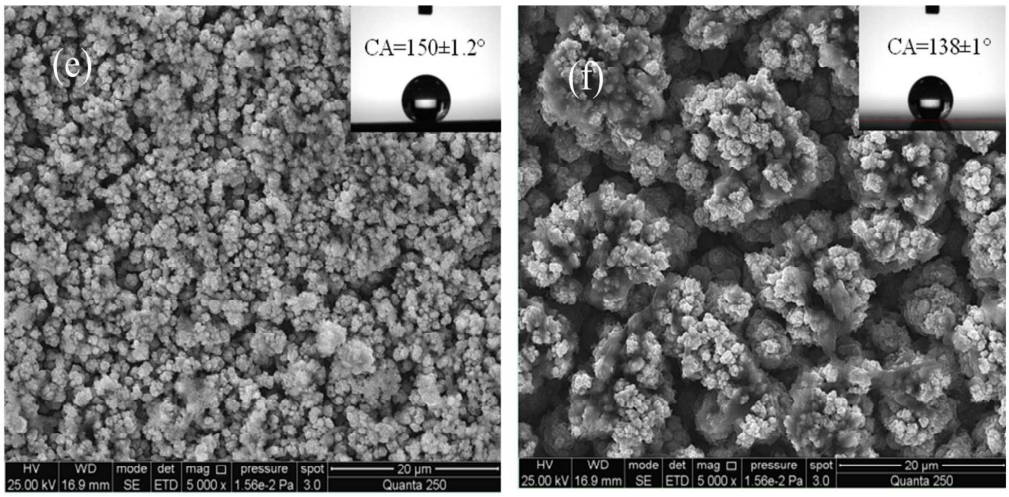

Fig.6.The coating morphology with different concentration of micro-TiO_2 particles.(at 5000× magnifications). (a) 0 g L^{-1}, (b) 5 g L^{-1}, (c) 10 g L^{-1}, (d) 20 g L^{-1}, (e) 30 g L^{-1}, (f) 40 g L^{-1}.

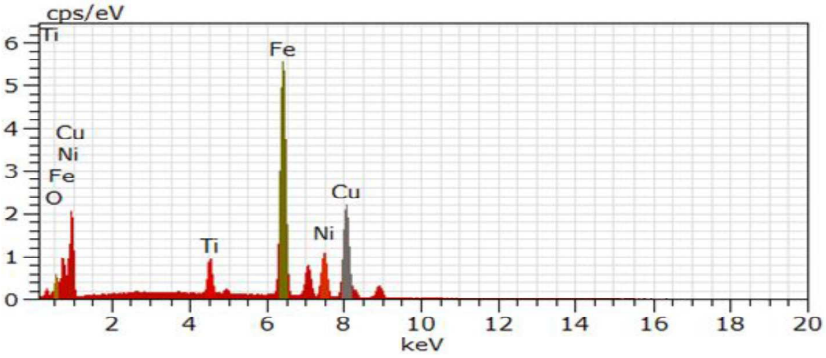

(A)

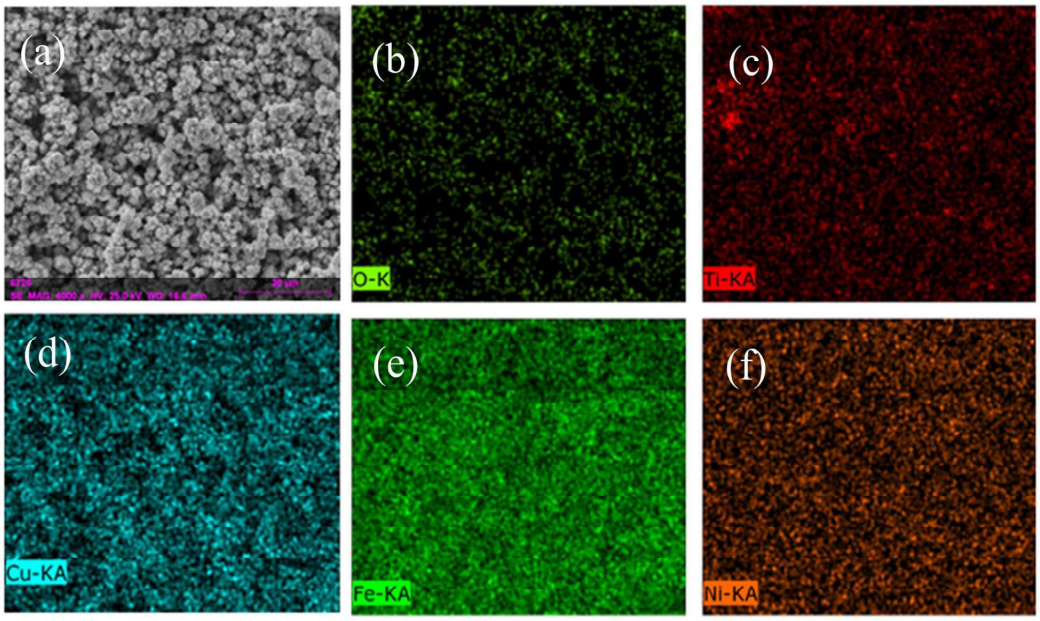

(B)

Fig.7. (A) EDS spectrum of optimal superhydrophobic coatings

(B) EDS map data of superhydrophobic coating chemical element distribution

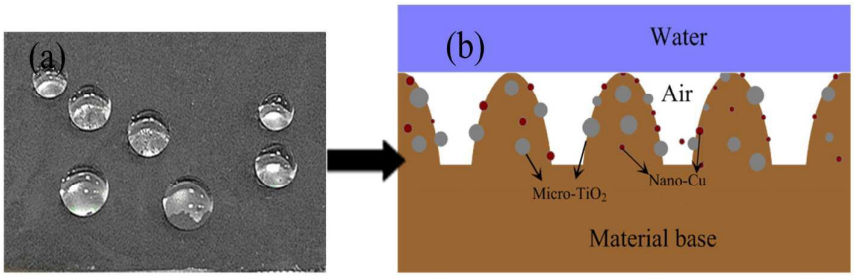

Fig.8. (a) optical image of water droplets of superhydrophobic coating and (b) simplified model of the coating surface with micro structure roughness

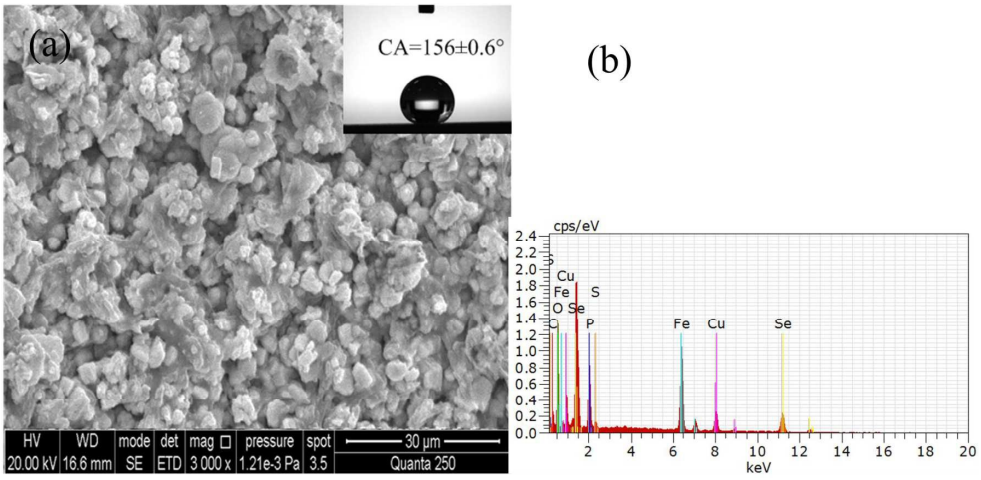

Fig.9. The morphology and EDS data of blackening treated coating

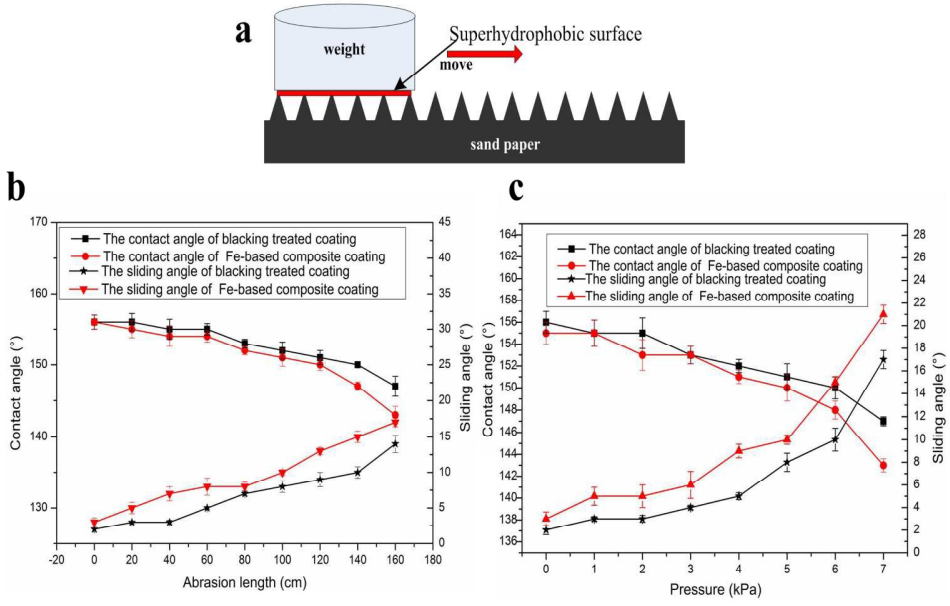

Fig.10. (a) the schematic diagram of scratch test, (b) the contact angle and sliding angle of different sample with different abrasion length under 4 kPa, and (c) the contact angle and sliding angle of different sample under different pressure after abrasion for 0.8 m.

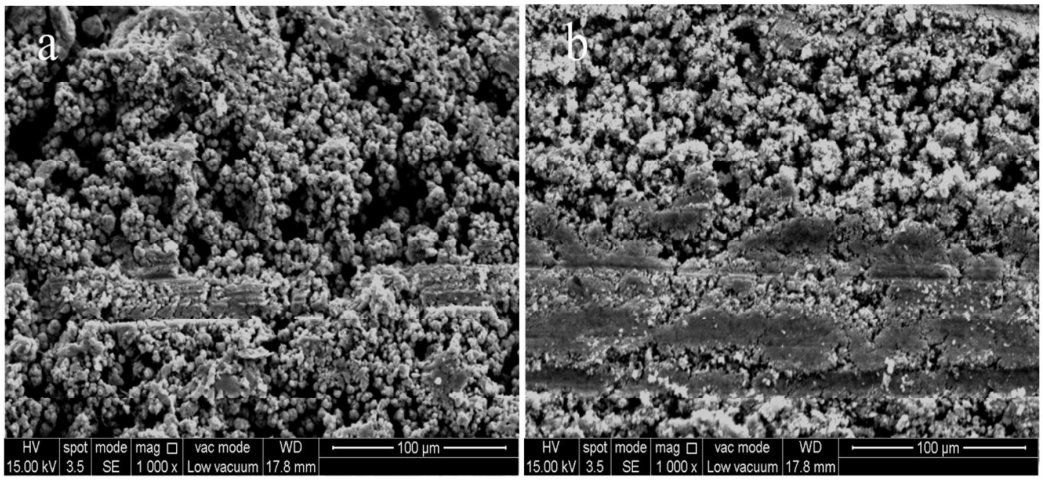

Fig.11. The SEM morphology of (a) Fe-based composite coating and (b) blacking treated Fe-based composite coating after abrasion for 1 m at applied pressure of 5 kPa.

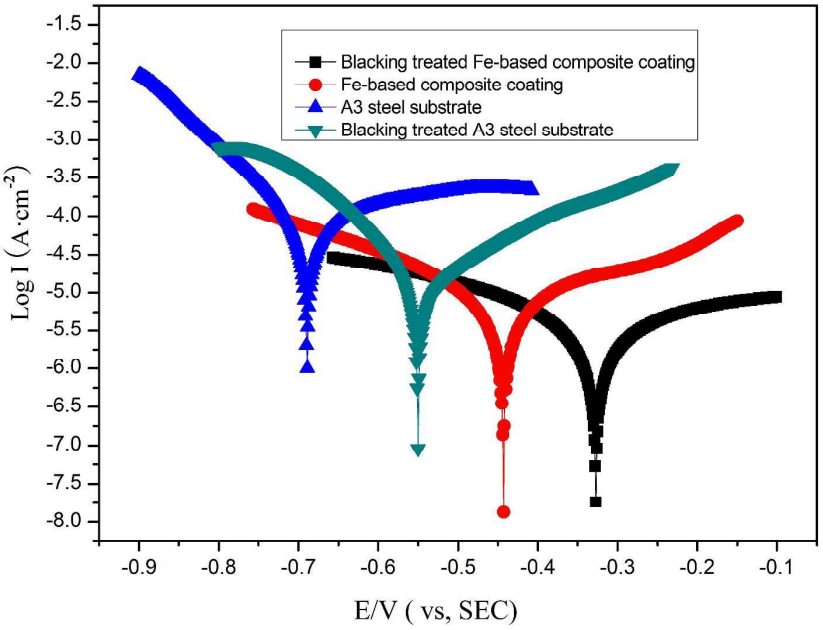

Fig.12. Potentiodynamic polarization curves of different process treated coatings

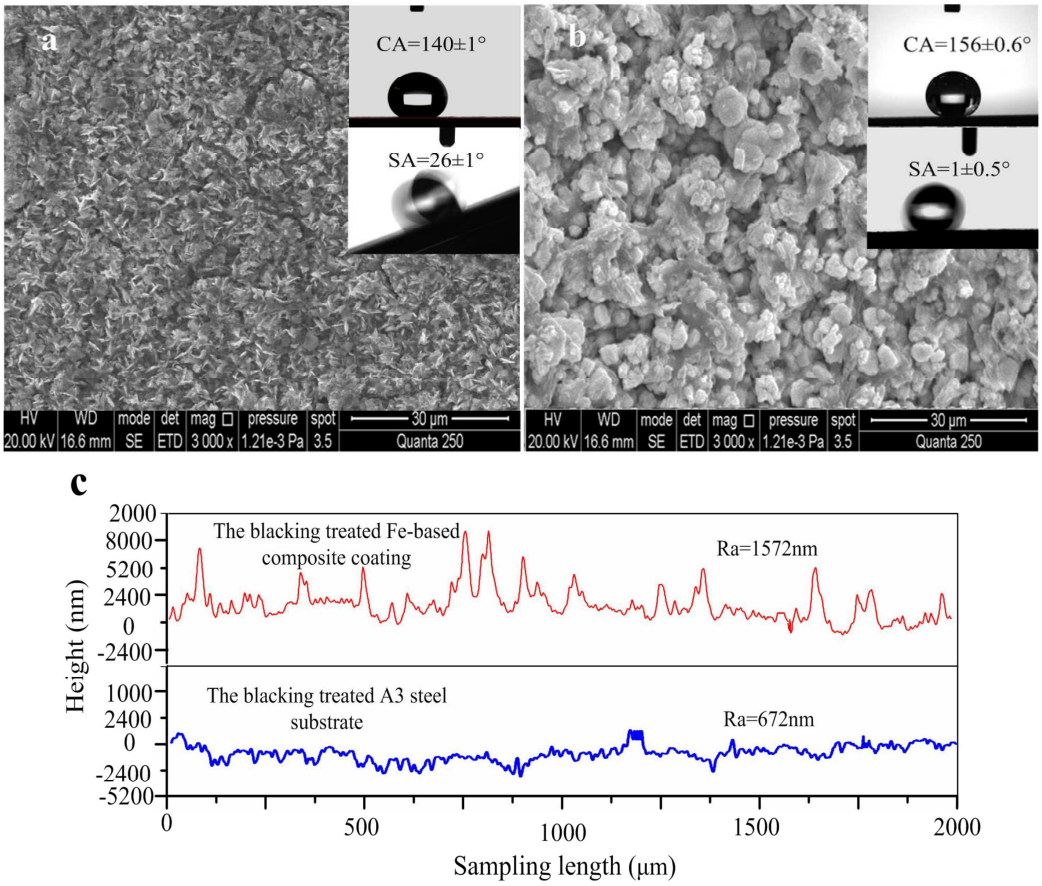

Fig.13.The SEM morphology of blacking treated (a) A3 steel substrate and (b) Fe-based composite coating, and the (c) surface roughness of the two samples.

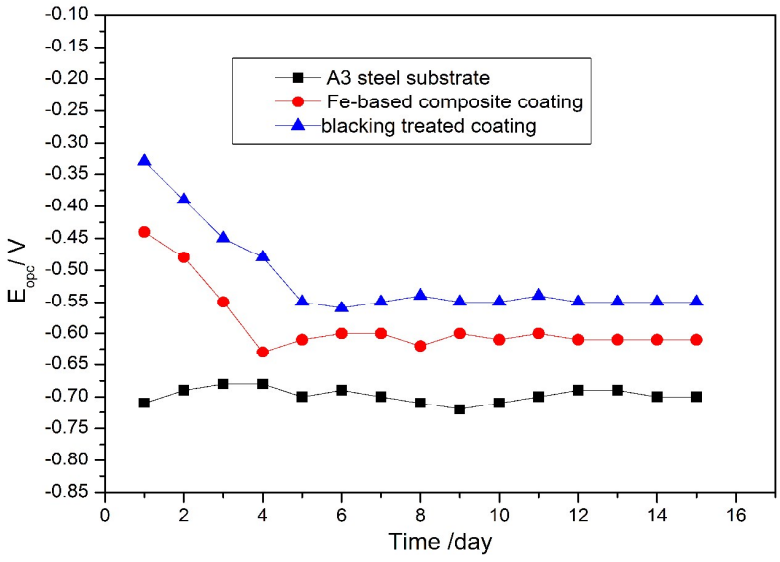

(A)

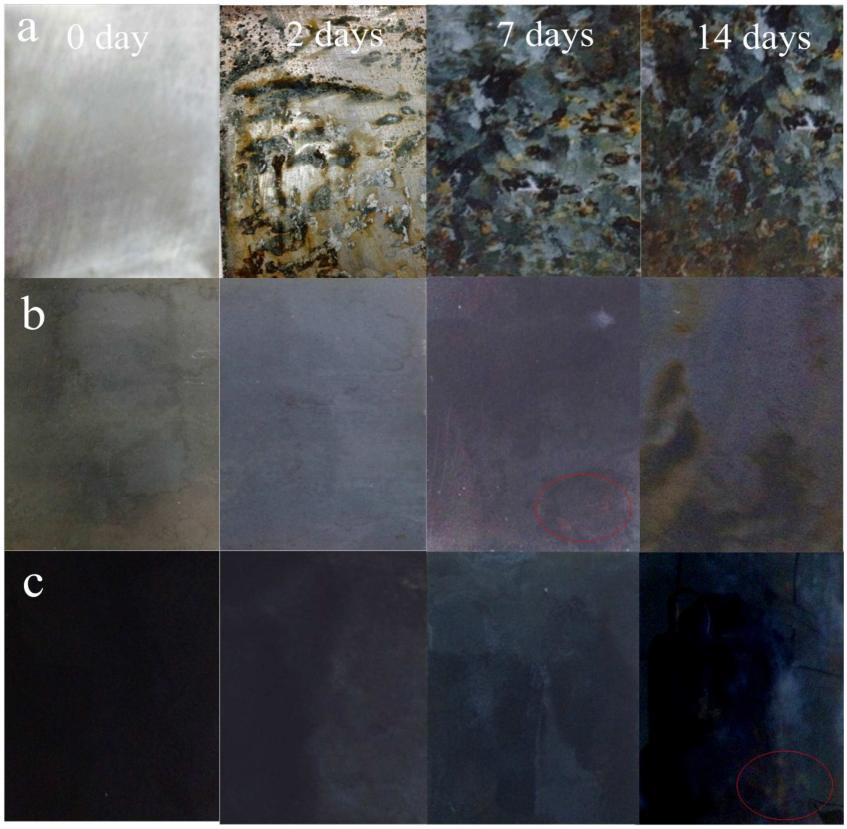

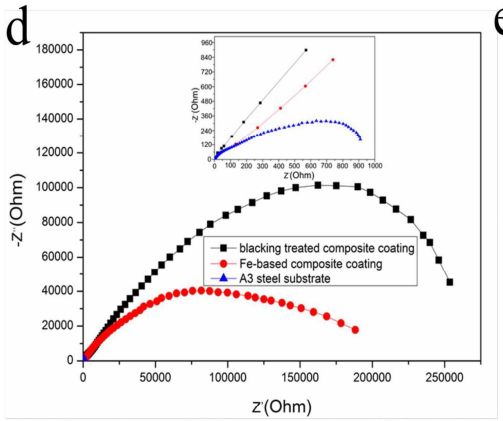

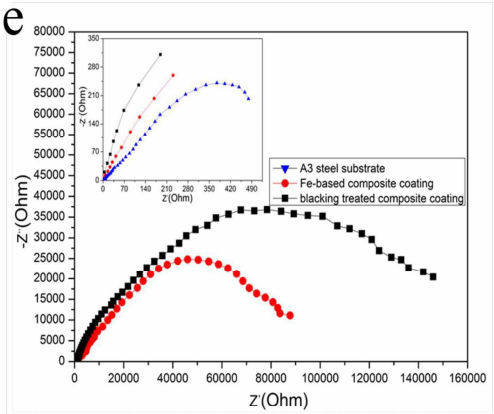

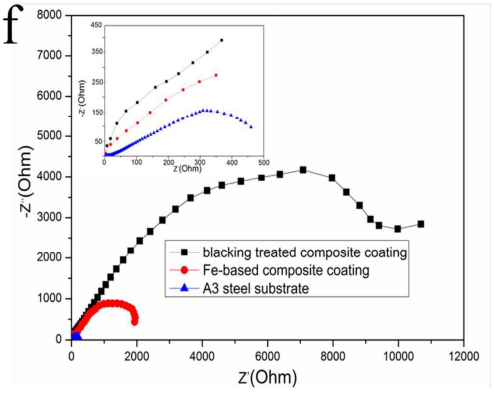

(B)

Fig.14 (A) The open circuit potential (OCP) of different samples versus time in 3.5% NaCl solution.

Fig.14 (B) The optical images of the (a)A3 steel substrate, (b)Fe-based composite coatings, (c)blacking treated composite surface after staying in 3.5% NaCl solution for several days and the Nyquist plots of different samples immersing for (d) 0 day, (e) 2days and(f)14days.

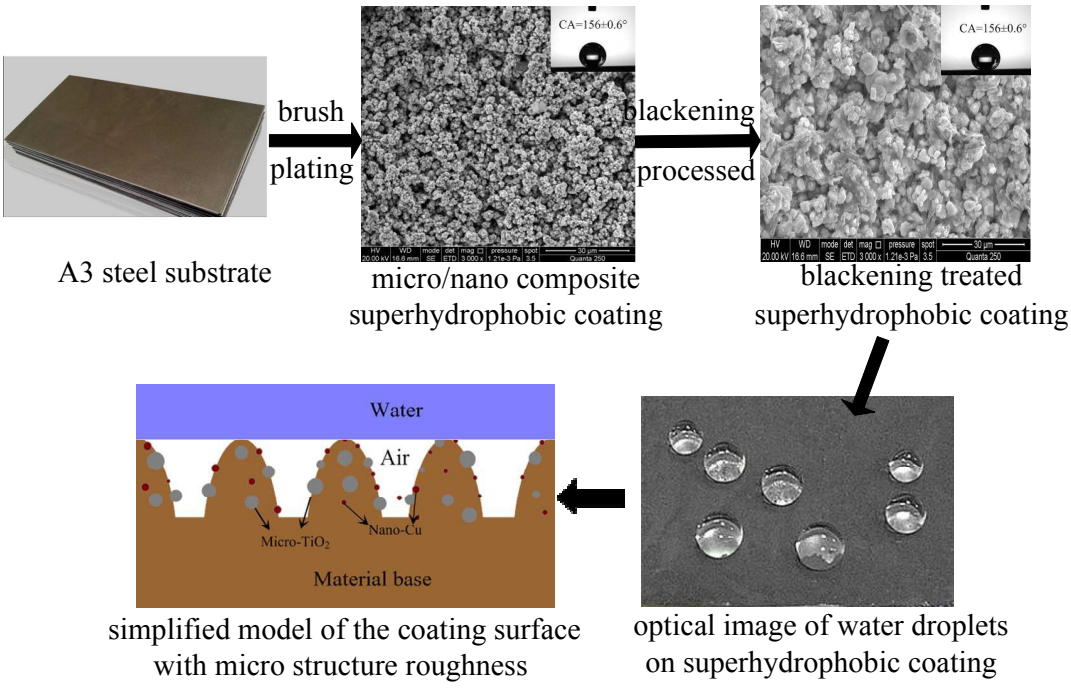

A3 steel substrate

micro/nano composite superhydrophobic coating

blackening treated superhydrophobic coating

simplified model of the coating surface with micro structure roughness

optical image of water droplets on superhydrophobic coating